Magnetic structure of hexagonal YMnO$_3$ and LuMnO$_3$ from a microscopic point of view

I. V. Solovyev[*]

Computational Materials Science Unit,

National Institute for Materials Science,

1-2-1 Sengen, Tsukuba, Ibaraki 305-0047, Japan

M. V. Valentyuk[†] and V. V. Mazurenko

Department of Theoretical Physics and Applied Mathematics,

Ural Federal University, Mira str. 19, 620002 Ekaterinburg, Russia

(Dated: March 4, 2013)

Abstract

The aim of this work is to unravel a basic microscopic picture behind complex magnetic properties of hexagonal manganites. For these purposes, we consider two characteristic compounds: $YMnO_3$ and $LuMnO_3$, which form different magnetic structures in the ground state ($P\underline{6}_3c\underline{m}$ and $P\underline{6}_3\underline{c}m$, respectively). First, we establish an electronic low-energy model, which describes the behavior of the Mn $3d$ bands of $YMnO_3$ and $LuMnO_3$, and derive parameters of this model from the first-principles calculations. From the solution of this model, we conclude that, despite strong frustration effects in the hexagonal lattice, the relativistic spin-orbit interactions lift the degeneracy of the magnetic ground state so that the experimentally observed magnetic structures are successfully reproduced by the low-energy model. Then, we analyze this result in terms of interatomic magnetic interactions, which were computed using different approximations (starting from the model Hamiltonian as well as directly from the first-principles electronic structure calculations in the local-spin-density approximation). We argue that the main reason why $YMnO_3$ and $LuMnO_3$ tend to form different magnetic structures is related to the behavior of the single-ion anisotropy, which reflects the directional dependence of the lattice distortion: namely, the expansion and contraction of the Mn-trimers, which take place in $YMnO_3$ and $LuMnO_3$, respectively. On the other hand, the magnetic coupling between the planes is controlled by the next-nearest-neighbor interactions, which are less sensitive to the direction of the trimerization. In the $P\underline{6}_3\underline{cm}$ structure of $YMnO_3$, the Dzyaloshinskii-Moriya interactions lead to the spin canting out of the hexagonal plane – in the same direction as the single-ion anisotropy. Finally, using the Berry-phase formalism, we evaluate the magnetic-state dependence of the ferroelectric polarization, and discuss potential applications of the latter in magnetoelectric switching phenomena.

I.   INTRODUCTION

Hexagonal manganites (the space group $P6_3cm$) are one of canonical examples of multiferroics, which have attracted an enormous attention recently. The coexistence of ferroelectricity and magnetism in such systems provides a unique possibility for manipulating the charges by applying a magnetic field and the spins by applying a voltage, which is crucially important for the construction of new forms of multifunctional devices.[1] To this end, the direct magnetic phase control by static electric field was realized in $HoMnO_3$.[2] The interplay between the ferroelectric activity and the magnetic order was also demonstrated in $YMnO_3$ and $LuMnO_3$ with the measurements of the dielectric constant and the loss tangent, which were shown to exhibit clear anomalies around the Néel temperature (T_N= 75 K and 88 K in $YMnO_3$ and $LuMnO_3$, respectively),[3,4] even despite the fact that the ferroelectric transition itself occurred at much higher temperature ($T_C \sim$ 880 K).[5] Another spectacular example is the coupling of magnetic and ferroelectric domains, which was visualized in $YMnO_3$ by using optical second harmonic generation technique.[6] Furthermore, the magnetic transition in $YMnO_3$ and $LuMnO_3$ is accompanied by a distinct change of the atomic positions.[7] Thus, the experimental data clearly demonstrates the existence of a strong coupling amongst electric, magnetic, and lattice degrees of freedom in these hexagonal manganites.

The magnetic frustration is one of the key concepts of multiferroic materials, which may assist the inversion symmetry breaking and, in a number of cases, be even responsible for such a breaking.[8] In this respect, the hexagonal lattice is not an exception, and is typically regarded as a playground for studying the magnetic frustration effects. However, it is also the main complication, hampering the theoretical understanding of multiferroic effects in hexagonal compounds, even despite the fact that the high-spin state (S=2), realized in manganites, is typically regarded as an "easy case" for such theoretical analysis, where the classical the spin fluctuations dominate over the quantum ones. Nevertheless, the ground state of classical spins in the hexagonal lattice is expected to be highly degenerate. Different signs of spin fluctuations, apparently originating from this degeneracy, were indeed observed in the neutron scattering experiments, even below T_N.[9,10] Another evidence of spin fluctuations, which is also related to the quasi-two-dimensional character of magnetic interactions, is the large ratio of the Curie-Weiss temperature (θ_{CW}) to T_N (about 7 in $YMnO_3$).[9]

The degeneracy can be lifted by lattice distortions and, in this context, plenty of attention

is paid to the so-called trimerization instability, inherent to the $P6_3cm$ structure.[7,11] However, the trimerization alone does not lift the frustration of isotropic exchange interactions. In this sense, the situation is fundamentally different from the exchange striction effect, which accompanies the formation of the E-type antiferromagnetic (AFM) state in the orthorhombic YMnO$_3$ and which lifts the frustration of nearest-neighbor (NN) interactions.[12] Nevertheless, the trimerization can interplay with the relativistic spin-orbit (SO) coupling and, in this way, give rise to new anisotropic interactions, which can lift the degeneracy and stabilize some individual magnetic structure with the well-defined symmetry. Such structures were detected in the experiments on the neutron diffraction (Ref. 11, 13, and 14) and optical second harmonic generation (Ref. 15). In a number of cases (e.g., in LuMnO$_3$), there can be several magnetic structures, coexisting in a narrow temperature range.[15] In short, despite difficulties, there is an enormous experimental progress in the identification of magnetic structures of hexagonal manganites, resulting from a delicate balance between lattice distortion, SO interaction, and frustration effects.

The microscopic understanding of rich magnetic properties of the hexagonal manganites is still rather limited. To begin with, there is no clear microscopic model, which would explain the origin of basic magnetic structures of hexagonal manganites, and why different manganites tend to form different magnetic structures. Basically, it is only known how the trimerization affects the NN isotropic interactions.[11] The presence of single-ion anisotropy and Dzyaloshinskii-Moriya (DM) interactions is, of course, anticipated. However, it is absolutely not clear how all these effects come together to form a variety of magnetic structures, realized in the hexagonal manganites.

In this paper, we will try to answer some of these questions. For these purposes, we consider two characteristic manganites: YMnO$_3$ and LuMnO$_3$, which form different magnetic structures in the ground state: $P6_3\underline{cm}$ and $P6_3\underline{cm}$, respectively (in the International notations, where each underlined symbol means that given symmetry operation is combined with the time inversion). We will show that this difference can be naturally related to different directions of the trimerization: expansion and contraction of the Mn-trimer, which takes place in YMnO$_3$ and LuMnO$_3$, respectively. In our study, we start from the first-principles electronic structure calculations. First, we construct a low-energy electronic model, which captures details of the magnetic structure and correctly reproduces the magnetic ground state of YMnO$_3$ and LuMnO$_3$. Then, we analyze these results by further transforming the

electronic model into the spin one and elucidating which magnetic interaction is responsible for each detail of the magnetic structure. We will also consider the 'temperature effect', associated with the temperature change of the experimental crystal structure, and show that above T_N it gradually diminishes the anisotropic interactions.

The rest of the paper is organized as follows. All methodological aspects, such as construction of the electronic model and calculation of magnetic interactions, are discussed in Sec. II. Results of solution of the electronic model in the Hartree-Fock (HF) approximation are presented in Sec. III A. In Sec. III B, we give a detailed analysis of the obtained results in terms of magnetic interactions, which were computed using different starting points. In Sec. III C, we discuss the magnetic part of the ferroelectric polarization and propose how it can be controlled by switching the magnetic state. Finally, a brief summary of the work is given in Sec. IV.

II. METHOD

Since our goal is the construction of microscopic theory for the magnetic properties of $YMnO_3$ and $LuMnO_3$, we first adopt the low-energy model, which would provide a realistic description for the Mn $3d$ bands of these compounds:

$$\hat{\mathcal{H}} = \sum_{ij} \sum_{\alpha\beta} t_{ij}^{\alpha\beta} \hat{c}_{i\alpha}^{\dagger} \hat{c}_{j\beta} + \frac{1}{2} \sum_{i} \sum_{\{\alpha\}} U_{\alpha\beta\gamma\delta} \hat{c}_{i\alpha}^{\dagger} \hat{c}_{i\gamma}^{\dagger} \hat{c}_{i\beta} \hat{c}_{i\delta}. \tag{1}$$

The model is constructed in the basis of Wannier orbitals, using the input from the first-principles electronic structure calculations. Each Wannier orbital is denoted by the Greek symbol, which itself is the combination of spin ($s= \uparrow$ or $\downarrow$) and orbital ($m= xy$, yz, $3z^2-r^2$, zx, or x^2-y^2) variables. Since the Mn $3d$ bands in hexagonal manganites are well separated from the rest of the spectrum,[11] the construction of the model Hamiltonian (1) is rather straightforward. The corresponding procedure can be found in Ref. 16.

All calculations have been performed using experimental parameters of the crystal structure, measured at 10 K and 300 K (Ref. 7, Supplementary Information), i.e. well below and above the magnetic transition point. The experimental space group $P6_3cm$ has 12 symmetry operations, which can be generated by the mirror reflection $x \rightarrow -x$, m_x, and the 60°-degree rotation around the z-axis, combined with the half of the hexagonal translation, $\{C_z^6|\mathbf{c}/2\}$.

The crystal-field splitting, obtained from the diagonalization of the site-diagonal part

of $\hat{t}_{ij} = \|t_{ij}^{\alpha\beta}\|$ (without spin-orbit coupling), is very similar in $YMnO_3$ and $LuMnO_3$. For example, if one uses the 10 K structure, we obtain the following scheme of the atomic levels: -0.54, -0.43, -0.29, -0.24, and 1.50 eV in the case of $YMnO_3$, and -0.60, -0.49, -0.25, -0.24, and 1.57 eV in the case of $LuMnO_3$. The use of the 300 K structure yields similar results. Clearly, the crystal field tends to stabilize four atomic orbitals, which are separated from the fifth one by the large energy gap. Such a scheme of the crystal-field splitting is consistent with the formal d^4 configuration of the Mn-ions, which is subjected to the Jahn-Teller instability. The fifth (unoccupied) orbital is of predominantly $3z^2 - r^2$ symmetry. The off-diagonal elements of $\hat{t}_{ij} = \|t_{ij}^{\alpha\beta}\|$ with respect to the site indices stand for the transfer integrals. They are listed in Ref. 17. The value of the screened Coulomb interaction U (defined as radial Slater's integral F^0) is about 2.6 eV for all considered systems. The intraatomic exchange (Hund's) coupling J_H is about 0.9 eV, which is practically unscreened. The full matrices of screened Coulomb interactions can be also found in Ref. 17.

After the construction, the model is solved in the HF approximation.[16] This procedure appears to be extremely useful, especially for the search of the magnetic ground state. Typically, in frustrated magnetic systems, we are dealing with the competition of several magnetic interactions of the both relativistic and non-relativistic origin. Therefore, even HF calculations for the relatively simple model (1) can be very time consuming, because they may require tends of thousands of iterations. In such a situation, the full scale electronic structure calculations are simply unaffordable. Since the degeneracy of the ground state is lifted by the lattice distortion, the HF approximation appears to be a good starting point for the analysis of the equilibrium magnetic properties.[16]

Of course, the model (1) is not perfect, because it does not explicitly include the oxygen band, which can be important for the quantitative analysis of magnetic properties of manganites. Therefore, whenever possible, we check results of our model analysis by direct calculations in the local-spin-density approximation (LSDA). For these purposes, we use the tight-binding linear muffin-tin-orbital method (in the following we will refer to such calculations as 'LMTO calculations').[18] Hopefully, in both cases we can employ the same strategy for calculations of magnetic interactions, which is based on the local force theorem and the Green's function technique. Namely, the isotropic exchange interactions (J_{ij}) can be obtained in the second order perturbation-theory expansion for the infinitesimal spin rotations,[19] antisymmetric DM interactions ($\mathbf{d}_{ij}$) – by considering mixed type perturba-

tion with respect to the rotations and the relativistic SO coupling,[20–22] and the single-ion anisotropy tensors $(\hat{\tau}_i)$ – in the second order with respect to the SO interaction[23].

The LMTO calculations have been performed for the AFM configuration ↑↓↑↓↑↓, where the arrows stand for the directions of magnetic moments at the sites 1-6 (see Fig. 1 for the notations of atomic positions). The use of the AFM configuration is essential in order
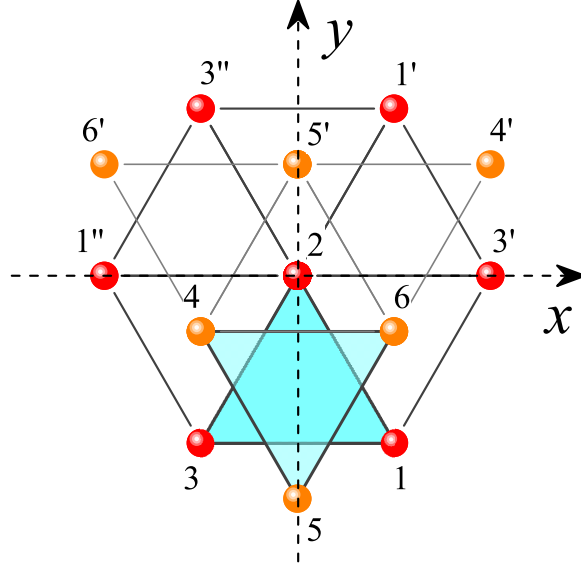

FIG. 1. (Color online) Relative positions of Mn-sites in the hexagonal $P6_3cm$ structure: the atoms located in the plane $z=0$ are indicated by the red (dark) spheres, and the atoms located in the plane $z=c/2$ are indicated by the light orange (grey) spheres. The Mn-trimers, which transform to each other by the symmetry operation $\{C_z^6|\mathbf{c}/2\}$, are shaded.

to open the band gap in LSDA (about 0.7 eV for YMnO$_3$, which is comparable with the experimental optical gap of 1.3 eV, reported in Ref. 24). Certain inconvenience of working with the AFM ↑↓↑↓↑↓ configuration is that it artificially lowers the $P6_3cm$ symmetry: in this case, the local symmetry can by preserved only around the sites 2 and 5, which will be selected as the reference points for the analysis of interatomic magnetic interactions.

In our LMTO calculations we decided to stick to the regular LSDA functional and not to use any corrections for the on-site Coulomb interactions (LSDA+U). On the one hand, such corrections can improve the description for interatomic magnetic interactions (similar to the model). On the other hand, the use of the LSDA+U functional is always conjugated with some additional uncertainties in the calculations, related to the double-counting problem.

Furthermore, the example of LaMnO$_3$ shows that LSDA is a reasonably good starting point for the analysis of interatomic magnetic interactions.[20] Nevertheless, when we compare the LMTO results with the model calculations we discuss possible consequences of the Coulomb U on the magnetic interactions in the former case.

Due to the hybridization with the oxygen states, which is treated explicitly in the LMTO calculations, the value of spin magnetic moment at the Mn-sites is reduced till 3.5 μ_B. Thus, some deviation of the local magnetic moment from the ionic value (4 μ_B), which is typically seen in the experiment,[11,13] can be attributed to the covalent mixing. In model HF calculations, similar effect can be described through the transformation from the Wannier basis to that of atomic orbitals.[16]

III.   RESULTS AND DISCUSSIONS

A.   Optimization of Magnetic Structure

We start with the central result of our work and argue that the low-energy model (1), with the parameters derived from the first-principles electronic structure calculations,[17] successfully reproduces the magnetic ground state of YMnO$_3$ and LuMnO$_3$.

The main candidates for the magnetic ground state of YMnO$_3$ and LuMnO$_3$ are shown in Fig. 2 (see also Refs. 13 and 14 for the notations). The unidimensional representations Γ_1, Γ_2, Γ_3, and Γ_4 correspond to the magnetic space groups $P6_3cm$, $P6_3\underline{cm}$, $P\underline{6}_3c\underline{m}$, and $P\underline{6}_3\underline{c}m$, respectively. The directions of the spin magnetic moment, obtained in the HF calculations for the low-energy model, are listed in Table I. In the Γ_1 and Γ_4 configurations, all magnetic moments lie in the xy-planes, while in the Γ_2 and Γ_3 configurations, there is also a small canting of magnetic moments along z. Moreover, the Γ_2 configuration allows for the weak ferromagnetism along z, while in the Γ_3 configuration, the z-components of the magnetic moments in the planes $z=0$ and $z=c/2$ cancel each other. More generally, the configurations Γ_1 (Γ_2) and Γ_4 (Γ_3) differ by the magnetic alignment in adjacent xy-planes: $\{C_z^6|\mathbf{c}/2\}$ acts as the normal symmetry operation in Γ_1 and Γ_2, which transforms these states to themselves, while in Γ_3 and Γ_4, $\{C_z^6|\mathbf{c}/2\}$ enters the magnetic symmetry group in the combination with the time-inversion operation $\hat{T}$. It corresponds to the additional flip of magnetic moments in the odd xy-planes of Γ_3 and Γ_4. We have also considered other
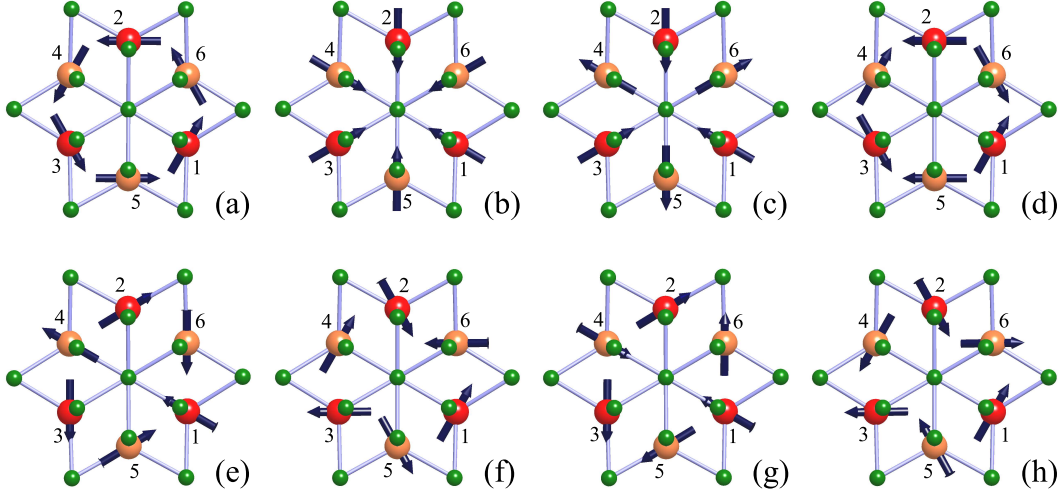
FIG. 2. (Color online) Magnetic structures obtained in the calculations (in the notations of Ref. 13): Γ_1 (a), Γ_2 (b), Γ_3 (c), Γ_4 (d), Γ_5 with $\mathbf{e}_1 \| [100]$ (e), Γ_5 with $\mathbf{e}_1 \| [120]$ (f), Γ_6 with $\mathbf{e}_1 \| [100]$ (g), and Γ_6 with $\mathbf{e}_1 \| [120]$ (h). The oxygen atoms are indicated by the small green (grey) spheres. The manganese atoms are indicated by the big spheres: the ones located in the $z = 0$ plane are shown by the red (dark) color, and the ones in the $z = c/2$ plane – by the light orange (grey) color.

possible magnetic configurations with the symmetries Γ_5 and Γ_6, as explained in Ref. 13. However, as it will become clear from the discussion below, they have higher energies.

The total energies of different magnetic configurations are summarized in Table II. Thus, the ground state of $YMnO_3$ is Γ_3 ($P\underline{6}_3c\underline{m}$), in agreement with the experiment.[11,15] In $LuMnO_3$, the ground state changes to Γ_4 ($P\underline{6}_3\underline{c}m$), also in agreement with the experiment.[11,15] However, all the states are located in a narrow energy range, which is expected for frustrated magnetic systems. The lower-symmetry magnetic structure $P\underline{6}_3$, which is typically regarded as another possible candidates for the magnetic ground state of the hexagonal manganites,[11,14,15] appears to be unstable and steadily converges to either $P\underline{6}_3c\underline{m}$ ($YMnO_3$) or $P\underline{6}_3\underline{c}m$ ($LuMnO_3$).

The band gap, obtained for both $YMnO_3$ and $LuMnO_3$, is about 2 eV, which is larger than experimental 1.3 eV.[24] Nevertheless, such a discrepancy is quite expectable for the level of the HF calculations.

TABLE I. The angles α and β, representing the directions $\mathbf{e}_i = (\cos\alpha_i\cos\beta_i, \cos\alpha_i\sin\beta_i, \sin\alpha_i)$ of the spin magnetic moments in the plane $z=0$, for different magnetic configurations (results of calculations using the experimental crystal structure, measured at 10 K). The atomic positions are explained in Fig. 1. For the magnetic configurations Γ_1, Γ_2, and Γ_6, the directions of the magnetic moments at the sites 4, 5, and 6 in the plane $z=c/2$ are obtained by the 180° rotations around the z-axis of the vectors $\mathbf{e}_1$, $\mathbf{e}_2$, and $\mathbf{e}_3$. For the magnetic configurations Γ_3, Γ_4, and Γ_5, these 180° rotations should be combined with the time inversion.

configuration	YMnO$_3$	LuMnO$_3$
Γ_1 and Γ_4	$\alpha_1 = 0,\ \beta_1 = 60°$	$\alpha_1 = 0,\ \beta_1 = 60°$
	$\alpha_2 = 0,\ \beta_2 = 180°$	$\alpha_2 = 0,\ \beta_2 = 180°$
	$\alpha_3 = 0,\ \beta_3 = 300°$	$\alpha_3 = 0,\ \beta_3 = 300°$
Γ_2 and Γ_3	$\alpha_1 = -0.2°,\ \beta_1 = 150°$	$\alpha_1 = -0.2°,\ \beta_1 = 150°$
	$\alpha_2 = -0.2°,\ \beta_2 = 270°$	$\alpha_2 = -0.2°,\ \beta_2 = 270°$
	$\alpha_3 = -0.2°,\ \beta_3 = 30°$	$\alpha_3 = -0.2°,\ \beta_3 = 30°$
Γ_5 with $\mathbf{e}_1\|[100]$	$\alpha_1 = -9.6°,\ \beta_1 = 150°$	$\alpha_1 = -8.8°,\ \beta_1 = 150°$
	$\alpha_2 = 4.8°,\quad \beta_2 = 30.5°$	$\alpha_2 = 4.4°,\quad \beta_2 = 30.3°$
	$\alpha_3 = 4.8°,\quad \beta_3 = 269.5°$	$\alpha_3 = 4.4°,\quad \beta_3 = 269.8°$
Γ_5 with $\mathbf{e}_1\|[120]$	$\alpha_1 = 0,\quad \beta_1 = 60°$	$\alpha_1 = 0,\quad \beta_1 = 60°$
	$\alpha_2 = -8.3°,\ \beta_2 = 299.5°$	$\alpha_2 = -7.6°,\ \beta_2 = 299.8°$
	$\alpha_3 = 8.3°,\quad \beta_3 = 180.5°$	$\alpha_3 = 7.6°,\quad \beta_3 = 180.3°$
Γ_6 with $\mathbf{e}_1\|[100]$	$\alpha_1 = -13.4°,\ \beta_1 = 150°$	$\alpha_1 = -23.3°,\ \beta_1 = 150°$
	$\alpha_2 = 6.6°,\quad \beta_2 = 30.8°$	$\alpha_2 = 11.4°,\quad \beta_2 = 30.1°$
	$\alpha_3 = 6.6°,\quad \beta_3 = 269.2°$	$\alpha_3 = 11.4°,\quad \beta_3 = 268.0°$
Γ_6 with $\mathbf{e}_1\|[120]$	$\alpha_1 = 0,\quad \beta_1 = 60°$	$\alpha_1 = 0,\quad \beta_1 = 60°$
	$\alpha_2 = -11.5°,\ \beta_2 = 299.2°$	$\alpha_2 = -20.2°,\ \beta_2 = 297.8°$
	$\alpha_3 = 11.5°,\quad \beta_3 = 180.8°$	$\alpha_3 = 20.2°,\quad \beta_3 = 182.2°$

B.   Analysis of Magnetic Interactions

In this section, we clarify results of the HF calculations for the low-energy model and argue that such a good agreement with the experimental data for the magnetic ground state is not

TABLE II. Total energies of different magnetic configurations as obtained in the Hartree-Fock calculations for the low-energy model. The energies are measured in meV per one formula unit, relative to the most stable configuration. The magnetic configurations are explained in Fig. 2. The calculations for $YMnO_3$ and $LuMnO_3$ have been performed using the experimental crystal structure, measured at 10 K and 300 K (as denoted in the notations).

configuration	$YMnO_3$ (10 K)	$YMnO_3$ (300 K)	$LuMnO_3$ (10 K)	$LuMnO_3$ (300 K)
Γ_1	0.37	0.20	0.48	0.23
Γ_2	0.16	0.19	0.61	0.32
Γ_3	0	0	0.13	0.10
Γ_4	0.21	0.01	0	0
Γ_5 with $\mathbf{e}_1\|[100]$	0.90	0.76	1.09	1.06
Γ_5 with $\mathbf{e}_1\|[120]$	0.90	0.76	1.09	1.06
Γ_6 with $\mathbf{e}_1\|[100]$	1.06	0.94	1.53	1.27
Γ_6 with $\mathbf{e}_1\|[120]$	1.06	0.94	1.53	1.27

surprising and can be understood from the analysis of corresponding magnetic interactions, which in turn depend on details of the lattice distortions in $YMnO_3$ and $LuMnO_3$. Thus, we consider the spin model:

$$\hat{\mathcal{H}}_S = -\sum_{\langle ij \rangle} J_{ij}\mathbf{e}_i\mathbf{e}_j + \sum_{\langle ij \rangle} \mathbf{d}_{ij}[\mathbf{e}_i \times \mathbf{e}_j] + \sum_i \mathbf{e}_i\hat{\tau}_i\mathbf{e}_i, \tag{2}$$

which can be obtained by eliminating the electronic degrees of freedom form the more general Hubbard model (1), or directly from the LMTO calculations.[16,19–23] In these notations, $\{J_{ij}\}$ are the isotropic exchange interactions, $\{\mathbf{d}_{ij}\}$ are the antisymmetric DM interactions, $\{\hat{\tau}_i\}$ are the single-ion anisotropy tensors, $\mathbf{e}_i$ stands the *direction* of the spin magnetic moment at the site i, and the summation runs over all *pairs* of atoms $\langle ij \rangle$.

The parameters of isotropic magnetic interactions are listed in Table III, and the atomic positions are explained in Fig. 1. All NN interactions in the plane xy are AFM. This is reasonable, because the ferromagnetic (FM) coupling in the hexagonal geometry can be stabilized only by virtual hoppings onto unoccupied $3z^2-r^2$ orbital, which are relatively small (see Ref. 17). Moreover, the number of orbital paths, available for the virtual hoppings via this particular $3z^2-r^2$ orbital, is also small. Nevertheless, from the orbital decomposition of

TABLE III. Parameters of isotropic exchange interactions (measured in meV), calculated in the ferromagnetic states of $YMnO_3$ and $LuMnO_3$. The atomic positions are explained in Fig. 1. Calculations have been performed using the experimental parameters of the crystal structure, measured at 10 K and 300 K (as denoted in the notations).

bond	$YMnO_3$ (10 K)	$LuMnO_3$ (10 K)	$YMnO_3$ (300 K)	$LuMnO_3$ (300 K)
2-1	-21.28	-31.81	-23.26	-30.16
2-1$'$	-26.35	-27.57	-22.67	-27.92
2-4	-0.12	-0.20	-0.13	-0.20
2-5$'$	-0.19	-0.11	-0.08	-0.10
2-4$'$	-0.24	-0.31	-0.21	-0.24
2-5	-0.07	-0.16	-0.16	-0.23

J_{ij} in our LMTO calculations, we can conclude that such a FM contribution does exists and compensates about 30 % of AFM contributions, involving all other orbitals, except $3z^2 - r^2$.

The symmetry of the $P6_3cm$ lattice is such that there are two types of NN interactions. The first type takes place in the triangles of atoms 1-2-3 (4-5-6), which are either expanded (the case of $YMnO_3$) or contracted (the case of $LuMnO_3$). The second type takes place in the bonds 2-1$'$, 2-3$'$, 2-1$''$, 2-3$''$, which are all equivalent. Then, due to the mirror reflection $x \rightarrow -x$, the NN bonds 2-4 and 2-6 between adjacent xy-planes are also equivalent, and differ from the bond 2-5$'$. The same situation holds for the next-NN interactions between the planes: there are two equivalent bonds 2-4$'$ and 2-6$'$, which differ from the bond 2-5. For the NN interactions, both in and between adjacent xy-planes, there is a clear correlation between the bondlength and the strength of the exchange coupling. For example, in the low-temperature structure of $YMnO_3$, the triangle of atoms 1-2-3 (4-5-6) is *expanded* (for two inequivalent NN bonds 2-1 and 2-1$'$ in the xy-plane, the ratio of the bondlengths is $l_{21'}/l_{21}=0.961$). Therefore, the AFM interaction $J_{21'}$ is stronger than J_{21}.[11] The same tendency holds for the interplane interactions: for two inequivalent NN bonds 2-5$'$ and 2-4 ($l_{25'}/l_{24}=0.991$), the AFM interaction $J_{25'}$ is stronger than J_{24}. In $LuMnO_3$, where the triangle of atoms 1-2-3 (4-5-6) is *compressed*, the situation is the opposite: $l_{21'}/l_{21}=1.016$ and $l_{25'}/l_{24}=1.003$. Therefore, the exchange interactions in the bonds 2-1 and 2-4 are stronger than in the bonds 2-1$'$ and 2-5$'$.

The behavior of next-NN interactions between the planes obeys quite different rules. Since the direct transfer integrals are small (see Ref. 17 for details), these interactions are realized as the "super-superexchange" processes via intermediate sites in the pathes 2→6→5, 2→1→5, etc., which always include one compressed and one expanded bond. Therefore, the simple analysis in terms of the bondlengths is no longer applicable. Instead, we have found that for all considered compounds (and all considered structures), the AFM interaction in the bond 2-5 appears to be weaker than in the bonds 2-4′ (and in the equivalent to it bond 2-6′). Such a behavior has very important consequences: in a noncollinear structure, it is more favorable energetically to form the FM coupling in the bond 2-5 in order to maximize the AFM coupling in two other next-NN bonds 2-4′ and 2-6′. Particularly, it explains why the magnetic ground state of $YMnO_3$ and $LuMnO_3$ should be Γ_3, Γ_4, or Γ_5, which are characterized by the FM coupling in the bond 2-5, and not Γ_1, Γ_2 or Γ_6, where this coupling is AFM (see Fig. 2). In $LuMnO_3$, this effect is additionally enhanced by the NN interactions between the planes: since AFM interaction in the bond 2-5′ is weaker than in two equivalent bonds 2-4 and 2-6, it is more favorable energetically to form the FM coupling between the sites 2, 5 and 5′, where the latter two are connected by the translation. However, in $YMnO_3$, the situation is the opposite and there is a strong competition between NN and next-NN interactions between the planes. Particularly, it explains a small energy difference between configurations Γ_3 and Γ_2.

The reliability of the obtained parameters can be checked by calculating θ_{CW}. In the case of classical Heisenberg model, the latter is given by the formula $\theta_{CW} \approx \sum_i J_{2i}/3k_B$, which yields -562 and -650 K for the 10 K structure of $YMnO_3$ and $LuMnO_3$, respectively. In the quantum case, these values should be additionally multiplied by $(1+1/S)$. The structural changes have some effect mainly on $YMnO_3$, and, if one uses parameters obtained for the 300 K structure, $|\theta_{CW}|$ decreases by 7% (for comparison, similar change of θ_{CW} for $LuMnO_3$ is about 1%). In any case, the obtained values are in a good agreement with experimental data.[4,7,11] The calculations of T_N are not straightforward: due to the quasi-two-dimensional character of isotropic exchange interactions, T_N will be strongly suppressed by thermal fluctuations, as one of the consequences of the Mermin-Wagner theorem.[25] Of course, the molecular-field approximation will overestimate T_N (by factor 4, in comparison with the experiment).

The LMTO calculations yield the following values of NN interactions in the plane xy

(in meV): $(J_{21}, J_{21'})= (-12.8, -19.6)$, $(-18.0, -17.0)$, $(-15.8, -16.6)$, and $(-17.0, -17.0)$ for YMnO$_3$ (10 K), LuMnO$_3$ (10 K), YMnO$_3$ (300 K), and LuMnO$_3$ (300 K), respectively. Thus, all the interactions are weaker than in the model analysis. Nevertheless, this seems reasonable. First, the NN interactions are generally weaker in the AFM ↑↓↑↓↑↓ configuration. This effect was also found in the model calculations, as will become clear below. Second, the ratio of AFM to FM contributions to the exchange coupling in manganites scales with the value of U as $(U-J_{\mathrm{H}})/(U+3J_{\mathrm{H}}) \approx 1-4J_{\mathrm{H}}/U$.[26] Thus, larger U, which was used in the model (but not in the LMTO calculations), will shift this balance towards the AFM coupling. Similar tendency was found for inter-layer interactions: although LSDA, supplementing the LMTO calculations, somewhat overestimates FM contributions to the exchange interactions, the modulation of these interactions, caused by the lattice distortion, again favors the formation of magnetic configurations Γ_3 or Γ_4. For example, in YMnO$_3$ (10 K), the LMTO calculations yield: $J_{24}= 0.20$ meV, $J_{25'}= 0.04$ meV, $J_{24'}= -0.14$ meV, and $J_{25}= 0.08$ meV. Therefore, these calculations confirm that the experimental coupling between hexagonal layers is stabilized by the next-NN interactions $J_{25} > J_{24'}$. The NN interactions act in the opposite direction: $J_{25'} < J_{24}$. However, their effect is smaller.

Let us discuss the behavior of the single-ion anisotropy tensor. Due to the mirror reflection $x\rightarrow-x$, the tensor $\hat{\tau}_2$ at the site 2 (see Fig. 1) has the following form:

$$
\hat{\tau}_2 = \begin{pmatrix} \tau^{xx} & 0 & 0 \\ 0 & \tau^{yy} & \tau^{yz} \\ 0 & \tau^{zy} & \tau^{zz} \end{pmatrix},
$$

where $\tau^{zy} = \tau^{yz}$ and $\tau^{xx}+\tau^{yy}+\tau^{zz} = 0$. Thus, the magnetic moments can either lie along the x-axis or be perpendicular to it. In the latter case (and if $\tau^{yz}\neq0$) they from a canted magnetic structure. The anisotropy tensors at other Mn-sites can be generated by applying the symmetry operations of the space group $P6_3cm$. The matrix elements of $\hat{\tau}_2$ can be evaluated in the second order of perturbation theory expansion with respect to the SO interactions.[23] Then, near the FM state, we obtain the following sets of independent parameters (in meV): $(\tau^{yy}, \tau^{yz}, \tau^{zz})= (-0.34, -0.12, 0.58)$, $(-0.29, -0.11, 0.58)$, $(-0.25, -0.12, 0.57)$, and $(-0.26, -0.12, 0.57)$ for YMnO$_3$ (10 K), YMnO$_3$ (300 K), LuMnO$_3$ (10 K), and LuMnO$_3$ (300 K), respectively. Since $\tau^{zz}>\tau^{yy}$, all structures with large z-components of the magnetic moments are energetically unfavorable. Then, by diagonalizing $\hat{\tau}_2$, one can find that the lowest-energy configuration in LuMnO$_3$ is the one where the magnetic moment at the site

14

2 is parallel to the x-axis. The next, canted magnetic configuration, is higher in energy by about 0.05 meV (for the 10 K structure). This situation is reversed in $YMnO_3$, where the lowest energy corresponds to the canted magnetic configuration. The angle α, formed by the magnetic moment and the y-axis, is about 7°. In the next configuration, which is higher in energy by about 0.10 meV (for the 10 K structure), the magnetic moment is parallel to the x-axis. This energy difference is reduced till 0.01 meV for the 300 K structure. The same behavior was found in the LMTO calculations: for $YMnO_3$, the lowest energy corresponds to the canted magnetic configuration (the canting from the y-axis is about 6°). The next configuration, where the magnetic moment is parallel to the x-axis, is higher in energy by 0.09 eV for the 10 K structure, and this energy difference further decreases for the 300 K structure.

Thus, the change of the ground state from Γ_3 to Γ_4 in the direction from $YMnO_3$ to $LuMnO_3$ is related to the behavior of the single-ion anisotropy, which in turns correlates with the distortion of the 1-2-3 triangles (expansion and contraction, respectively). Moreover, due to the 180° rotation around the z-axis, which is required in order to transform the site 2 to the site 5 (see Fig. 1), the matrix element τ^{yz} will change sign. Therefore, the canting of spins in the planes $z=0$ and $z=c/2$ of the Γ_3 structure will act in the opposite directions, and the magnetic moments along the z-axis will cancel each other.

The single-ion anisotropy will tend to align z-components of the magnetic moments ferromagnetically in each of the xy-plane. However, this effect will compete with the NN AFM interactions J_{21} and $J_{21'}$. The corresponding analytical expression for the spin canting can be obtained by minimizing the energies of single-ion anisotropy and isotropic exchange interactions: by assuming that all neighboring spins in the xy-plane form the 120°-structure (as in the case of the Γ_2 and Γ_3 configurations), one can find that

$$\tan 2\alpha = -\frac{2\tau^{yz}}{\tau^{yy} - \tau^{zz} + 3J_{21} + 6J_{21'}}, \tag{3}$$

where the minus-sign corresponds to the situation, which is realized in our HF calculations and where $\mathbf{e}_2$ is antiparallel to the y-axis (see Fig. 2). Then, for the Γ_3 configuration of $YMnO_3$ (10 K), the canting angle α can be estimated (using both model and LMTO parameters of magnetic interactions) as $\alpha \approx -\tau^{yz}/(3J_{21} + 6J_{21'}) = -0.03°$, which is about 7 times smaller than the values obtained in self-consistent HF calculations (Table I). Nevertheless, there is an additional contribution to the spin canting, caused by the DM interactions.

Parameters of DM interactions between NN sites in the xy-plane are listed in Table IV. They were obtained by considering mixed perturbation theory expansion with respect to

TABLE IV. Parameters of Dzyaloshinskii-Moriya interactions (measured in meV), calculated in the ferromagnetic states of YMnO$_3$ and LuMnO$_3$. The atomic positions are explained in Fig. 1. Calculations have been performed using the experimental parameters of the crystal structure, measured at 10 K and 300 K (as denoted in the notations).

bond	YMnO$_3$ (10 K)	LuMnO$_3$ (10 K)	YMnO$_3$ (300 K)	LuMnO$_3$ (300 K)
2-1	$(0.01, 0.01, 0.20)$	$(0.04, 0.02, 0.25)$	$(0.04, 0.02, 0.17)$	$(0.07, 0.04, 0.25)$
2-1'	$(0.03, -0.02, 0.21)$	$(0.03, -0.02, 0.26)$	$(0.03, -0.01, 0.18)$	$(0.02, -0.01, 0.26)$
2-1''	$(0, 0.04, 0.21)$	$(-0.01, 0.04, 0.26)$	$(0, 0.03, 0.18)$	$(0, 0.02, 0.26)$

the SO interaction and infinitesimal rotations of spin magnetic moments.[20] In principle, the parameters $\mathbf{d}_{21'}$ and $\mathbf{d}_{21''}$ are not independent and can be transformed to each other using symmetry operations of the space group $P6_3cm$. However, it is more convenient to consider their contributions independently. Due to the mirror reflection $x \to -x$, the elements of two *axial* vectors $\mathbf{d}_{23}$ and $\mathbf{d}_{21}$ (see Fig. 1) obey the following rules: $d_{23}^x = d_{21}^x$, $d_{23}^y = -d_{21}^y$, and $d_{23}^z = -d_{21}^z$ (similar situation holds for other NN interactions). Thus, they will produce a finite canting at the site 2 only if the directions of two other magnetic moments $\mathbf{e}_2$ and $\mathbf{e}_3$ would have an AFM component along x and a FM component along y, i.e.: $e_3^x = -e_1^x$ and $e_3^y = e_1^y$. Such a situation is realized in the magnetic configurations Γ_2 and Γ_3 (but not in Γ_1 and Γ_4). Then, the magnetic moment at the site 2 will experience the additional rotational force from the sites 1, 1', and 1'': $\mathbf{f}_{1 \to 2} = [\mathbf{d}_{21} \times \mathbf{e}_1] + [\mathbf{d}_{21'} \times \mathbf{e}_1] + [\mathbf{d}_{21''} \times \mathbf{e}_1]$. For the magnetic configurations Γ_2 and Γ_3, the sites of the type '3' will create the same rotational force: $\mathbf{f}_{3 \to 2} = \mathbf{f}_{1 \to 2}$. However, for the Γ_1 and Γ_4 configurations, it holds $\mathbf{f}_{3 \to 2} = -\mathbf{f}_{1 \to 2}$. Therefore, these two contribution will cancel each other and there will be no canting of spins.

These rotational forces should be incorporated in the expression (3) for the spin canting, which yields $\alpha \approx -(\tau^{yz} + f_{1 \to 2}^z)/(3J_{21} + 6J_{21'}) = -0.04°$. This canting is still smaller than $\alpha \sim -0.21°$, obtained in the HF calculations for the Γ_3 configuration (Table I). Nevertheless, it should be noted that all the parameters of the spin Hamiltonian (2) were evaluated using perturbation theory expansion near the collinear FM state, which is very far from the ground-state configuration Γ_3. Thus, it is difficult to expect that the perturbation theory, although

is very useful for the semi-quantitative analysis, should be able to reproduce all details of the solutions of the electronic model (1). In fact, some parameters of the spin Hamiltonian (2) appear to be sensitive to the state, in which they are calculated. For example, we have also considered the collinear AFM configuration ↑↓↑↓↑↓, where the arrows stand for the directions of magnetic moments at the sites 1-6. In this case, the DM interactions involving the site 2, which is AFM coupled with all NN spins in the xy-plane, become (in meV): $\mathbf{d}_{21} = (0.01, 0.03, 0.01)$, $\mathbf{d}_{21'} = (0.04, 0, 0)$, and $\mathbf{d}_{21''} = (-0.01, 0.05, 0.01)$. Then, corresponding rotational force $f_{1\rightarrow 2}^z$ will be about 2 times larger than in the FM state. Meanwhile, the parameters of isotropic exchange interactions J_{21} and $J_{21'}$ decrease by about 15%. These factors will additionally increase α.

Furthermore, the HF potential for the low-energy model (1) is orbitally dependent. In this cases, the local force theorem is no longer valid.[19] Therefore, the total energy change due to the SO interaction can be replaced only approximately by the change of the single-particle energies of the HF method. For the single-ion anisotropy, the situation was discussed in Appendix B of Ref. 23. Presumably, this is the main reason, explaining the quantitative difference between the results of the electronic and spin models. Thus, these are typical uncertainties, supplementing the construction and analysis of the spin model (2).

Nevertheless, the local force theorem is valid within LSDA. Therefore, it is interesting to estimate the spin canting in the LMTO calculations, which are based on the LSDA functional. In this case, all DM interactions become larger. For example, for YMnO$_3$ (10 K) we have obtained the following parameters (in meV): $\mathbf{d}_{21} = (-0.01, 0.14, -0.20)$, $\mathbf{d}_{21'} = (-0.16, 0.04, -0.12)$, and $\mathbf{d}_{21''} = (0.06, 0.18, -0.26)$. Then, by combining them with corresponding parameters of the single-ion anisotropy $\tau^{yz} = -0.078$ meV and isotropic exchange interactions J_{21} and $J_{21'}$, which are listed above, we obtain the canting angle $\alpha = -0.12°$. Thus, it is interesting that LSDA, despite its limitation, provides the best starting point for the analysis of the spin canting via the perturbation-theory expansion for the spin-orbit interaction, due to validity of the local force theorem. Similar situation was found in the orthorhombic LaMnO$_3$.[20]

Thus, although derivation of parameters of spin model (2) may differ in details, depending on the form of the electronic Hamiltonian, which is used as the starting point, as well as some additional approximations, underlying definitions of the model parameters, this analysis provides a clear microscopic basis for understanding the main difference between YMnO$_3$

and LuMnO$_3$: why the former tends to form the canted noncollinear magnetic structure Γ_3, while the latter forms the planar structure Γ_4.

C. Magnetic Contribution to Ferroelectric Polarization

Finally, we would like to comment on the behavior of electronic polarization $\mathbf{P}||\mathbf{c}$. It was calculated within the Berry-phase formalism,[27] which was adopted for the model calculations.[8] Of course, the ferroelectric activity in YMnO$_3$ and LuMnO$_3$ is primarily caused by structural effects. For example, in YMnO$_3$, the ferroelectric transition occurs at about $T_C = 880$ K,[5] which is much higher than $T_N = 75$ K.[7] This fact was also confirmed by first-principles calculations.[28] Another appealing evidence is that the ferroelectric domains in YMnO$_3$ always coincide with the structural ones.[5] Nevertheless, beside this structural deformation, we have found that there is a substantial magnetic contribution to $\mathbf{P}||\mathbf{c}$. More specifically, all magnetic configurations can be divided in two group. The first one includes Γ_1, Γ_2, and Γ_6, where the magnetic moments in the planes $z=0$ and $z=c/2$ can be transformed to each other by the simple rotations. The second groups includes Γ_3, Γ_4, and Γ_5, where these rotations should be additionally combined with the time inversion. According to our finding, the states in each group are characterized by nearly equal values of $\mathbf{P}||\mathbf{c}$. However, the transformation of the magnetic state from one group to another would cause a finite jump of electronic polarization. Thus, in principle, the value of the ferroelectric polarization can be controlled by changing the magnetic state (and vice versa). In this sense, more promising candidate is YMnO$_3$, where the ground state (Γ_3) and the first excited state (Γ_2) belong to different groups. The energy difference ΔE between these two configurations is about 0.16 meV (see Table II). Then, the change of the ferroelectric polarization, associated with the change of the magnetic state $\Gamma_3 \rightarrow \Gamma_2$, can be estimated as $\Delta \mathbf{P}||\mathbf{c} = -120$ μC/m^2. The practical realization of such a switching phenomenon would be probably interesting, although it is not immediately clear, which external interaction could switch the magnetic state. Formally speaking, the magnetic configuration Γ_2 could be stabilized by the external electric field $\mathbf{E}||\mathbf{c}$, which couples to $\Delta \mathbf{P}$ and results in the additional energy gain $-\Delta \mathbf{P}\mathbf{E}$. Alternatively, one could exploit the fact that Γ_2 allows for a weak ferromagnetism along z (while Γ_3 does not) and, therefore, could be also stabilized by interaction with the external magnetic field, $-\Delta \mathbf{M}\mathbf{B}$, which couples to the net magnetic

moment $\Delta \mathbf{M}$ ($\sim -0.01\mu_B$ per Mn-site). However, in order to overcome the total energy difference ΔE, this would require unrealistically large values of $\mathbf{E}$ and $\mathbf{B}$, which cannot be realized in practice. Therefore, one should explore alternative possibilities. For example, from the viewpoint of microscopic interactions, one could use the competition of the NN and next-NN interactions between adjacent xy-planes, which in the case of YMnO$_3$ act in the *opposite* direction (see discussions above). The Γ_3 configuration is stabilized by the next-NN interactions. However, if one could find such macroscopic conditions, which would shift this balance towards NN interactions, one could switch the magnetic structure $\Gamma_3 \to \Gamma_2$ and, therefore, the ferroelectric polarization. Another possibility is, of course, to exploit magnetism of the rare-earth ions, which can act similar to $\mathbf{B}$, but produces much stronger effect on the Mn-sublattice. Such a magnetic phase control was indeed realized experimentally in the series of hexagonal manganites with the magnetic rare-earth sublattices.[2,29]

IV. SUMMARY

Using results of first-principles electronic structure calculations, we have established the low-energy model, which is able to capture basic magnetic properties of hexagonal manganites. This Hubbard-type model describes the behavior of the Mn $3d$ bands, being subjected to the lattice deformation and on-site electron-electron interactions. All parameters of such model, derived from the first principles calculations for two characteristic manganites YMnO$_3$ and LuMnO$_3$, are summarized in Ref. 17.

Then, the model was solved in the HF approximation, by considering all possible non-collinear magnetic structures with different symmetries. Since the magnetic frustration in the hexagonal $P6_3cm$ lattice is lifted by the relativistic SO interaction, the HF approximation provides a good starting point for the analysis of the magnetic properties of these compounds and successfully reproduce the experimental change of the magnetic ground state from $P\underline{6}_3\underline{cm}$ to $P\underline{6}_3\underline{cm}$ in the direction from YMnO$_3$ to LuMnO$_3$, which was observed in the neutron diffraction and nonlinear optical studies.

In order to clarify the microscopic origin of such a change, we have further transformed the electronic model into the spin one and discussed the same trend in terms of differences in the behavior of magnetic interactions in these systems. We have found that the main reason why YMnO$_3$ and LuMnO$_3$ tend to form different magnetic structure is related to

the behavior of the single-ion anisotropy, which couples to the trimerization distortion in the hexagonal plane and reflects different directions of this trimerization in YMnO$_3$ and LuMnO$_3$ (expansion and construction of the Mn-trimers, respectively). On the other hand, the interplane coupling in both compounds is controlled by the next-NN interactions, which is less sensitive to the direction of trimerization. The spin canting in the $P\underline{6}_3c\underline{m}$ structure of YMnO$_3$ is a combined effect of both single-ion anisotropy and Dzyaloshinskii-Moriya interactions, which act in the same direction. As the trimerization distortion decreases with the temperature, all anisotropic interactions also decrease, thus reviving the magnetic frustration and the degeneracy of the magnetic state.

Finally, using the Berry-phase formalism, we have estimated the magnetic contribution to the ferroelectric polarization and discussed how it can be controlled by changing the magnetic structure of YMnO$_3$.

---

* SOLOVYEV.Igor@nims.go.jp

† Temporarily at Institute of Theoretical Physics, University of Hamburg, Jungiusstrasse 9, 20355 Hamburg, Germany

1 S.-W. Cheong and M. Mostovoy, Nature Materials **6**, 13 (2007).

2 Th. Lottermoser, Th. Lonkai, U. Amann, D. Hohlwein, Jörg, and M. Fiebig, Nature **430**, 541 (2004).

3 Z. J. Huang, Y. Cao, Y. Y. Sun, Y. Y. Xue, C. W. Chu, Phys. Rev. B **56**, 2623 (1997).

4 T. Katsufuji, S. Mori, M. Masaki, Y. Moritomo, N. Yamamoto, and H. Takagi, Phys. Rev. B **64**, 104419 (2001).

5 T. Choi, Y. Horibe, H. T. Yi, Y. J. Choi, W. Wu, and S.-W. Cheong, Nature Materials **9**, 253 (2010).

6 M. Fiebig, Th. Lottermoser, D. Frölich, A. V. Goltsev, and R. V. Pisarev, Nature **419**, 818 (2002).

7 S. Lee, A. Pirogov, M. Kang, K.-H. Jang, M. Yonemura, T. Kamiyama, S.-W. Cheong, F.

Gozzo, N. Shin, H. Kimura, Y. Noda, and J.-G. Park, Nature **451**, 805 (2008).

[8] I. V. Solovyev and Z. V. Pchelkina, Phys. Rev. B **82**, 094425 (2010); I. V. Solovyev, *ibid.* **83**, 054404 (2011). Note that a prefactor was missing in the previous model calculations of **P**, and all values of the electric polarization, reported in this paper, should be additionally divided roughly by 2.5. This partly resolves the problem of disagreement with the experimental data. The details will be discussed in a separate publication.

[9] J. Park, J.-G. Park, G. S. Jeon, H.-Y. Choi, C. Lee, W. Jo, R. Bewley, K. A. McEwen, and T. G. Perring, Phys. Rev. B **68**, 104426 (2003).

[10] T. J. Sato, S.-H. Lee, T. Katsufuji, M. Masaki, S. Park, J. R. D. Copley, and H. Takagi, Phys. Rev. B **68**, 014432 (2003).

[11] J. Park, S. Lee, M. Kang, K.-H. Jang, C. Lee, S. V. Streltsov, V. V. Mazurenko, M. V. Valentyuk, J. E. Medvedeva, T. Kamiyama, and J.-G. Park, Phys. Rev. B **82**, 054428 (2010).

[12] D. Okuyama, S. Ishiwata, Y. Takahashi, K. Yamauchi, S. Picozzi, K. Sugimoto, H. Sakai, M. Takata, R. Shimano, Y. Taguchi, T. Arima, and Y. Tokura, Phys. Rev. B **84**, 054440 (2011).

[13] A. Muñoz, J. A. Alonso, M. J. Martínez-Lope, M. T. Casáis, J. L. Martínez, and M. T. Fernández-Díaz, Phys. Rev. B **62**, 9498 (2000).

[14] P. J. Brown and T. Chatterji, J. Phys.: Condens. Matter **18**, 10085 (2006).

[15] M. Fiebig, D. Frölich, K. Kohn, St. Leute, Th. Lottermoser, V. V. Pavlov, and R. V. Pisarev, Phys. Rev. Lett. **84**, 5620 (2000).

[16] I. V. Solovyev, J. Phys.: Condens. Matter **20**, 293201 (2008).

[17] Supplemental materials [parameters of the crystal field, transfer integrals, and matrices of Coulomb interactions].

[18] O. K. Andersen, Z. Pawlowska, and O. Jepsen, Phys. Rev. B **34**, 5253 (1986).

[19] A. I. Liechtenstein, M. I. Katsnelson, V. P. Antropov, and V. A. Gubanov, J. Magn. Magn. Matter. **67** 65 (1987).

[20] I. Solovyev, N. Hamada, and K. Terakura, Phys. Rev. Lett. **76**, 4825 (1996).

[21] V. V. Mazurenko and V. I. Anisimov, Phys. Rev. B **71**, 184434 (2005). Note that this work employed the same strategy for derivation of parameters of DM interactions as in Ref. 20, but different choice of phases in the spin-rotation matrix. Namely, the rotation of spin from $\mathbf{e}^0 = (0,0,1)$ to $\mathbf{e} = (\cos\varphi\sin\theta, \sin\varphi\sin\theta, \cos\theta)$ was described by the following sets of the Euler angles: $(\alpha_I, \beta_I, \gamma_I) = (\varphi, \theta, -\varphi)$, in this work, and $(\alpha_{II}, \beta_{II}, \gamma_{II}) = (\varphi, \theta, 0)$, in Ref. 20.

The second choice provides more compact expression for DM interactions and allows to get rid of the on-site contribution to the rotational force. Of course, the total force, created by all spins, does not depend on the phase choice.

[22] A. N. Rudenko, V. V. Mazurenko, V. I. Anisimov, A. I. Lichtenstein, Phys. Rev. B **79**, 144418 (2009).

[23] I. V. Solovyev, P. H. Dederichs, and I. Mertig, Phys. Rev. B **52**, 13419 (1995).

[24] A. M. Kalashnikova and R. V. Pisarev, JETP Letters **78**, 143 (2003).

[25] N. D. Mermin and H. Wagner, Phys. Rev. Lett. **17**, 1133 (1966); *ibid.* **17**, 1307(E) (1966).

[26] K. I. Kugel and D. I. Khomskii, Sov. Phys. Usp. **25**, 231 (1982).

[27] D. Vanderbilt and R. D. King-Smith, Phys. Rev. B **48**, 4442 (1993); R. Resta, J. Phys.: Condens. Matter **22**, 123201 (2010).

[28] B. B. van Aken, T. T. M. Palstra, A. Filippetti, and N. A. Spaldin, Nature Materials **3**, 164 (2004).

[29] M. Fiebig, Th. Lottermoser, and R. V. Pisarev, J. Appl. Phys. **93**, 8194 (2003).